Laser and Particle Beams (2017), *35*, 442–449.

doi:10.1017/S026303461700043X

Experimental and numerical study of ultra-short laser-produced collimated Cu K_α X-ray source

R. RATHORE,[1,*] V. ARORA,[1] H. SINGHAL,[1] T. MANDAL,[1,2] J.A. CHAKERA,[1,2] AND P.A. NAIK[1,2]

[1]Laser Plasma Section, Raja Ramanna Centre for Advanced Technology, Indore 452013, Madhya Pradesh, India
[2]Homi Bhabha National Institute, Anushaktinagar, Mumbai 400 094, Maharashtra, India

(Received 10 March 2017; Accepted 30 May 2017)

Abstract

K_α X-ray sources generated from the interaction of ultra-short laser pulses with solids are compact and low-cost source of ultra-short quasi-monochromatic X-rays compared with synchrotron radiation source. Development of collimated ultra-short K_α X-ray source by the interaction of 45 fs Ti:sapphire laser pulse with Cu wire target is presented in this paper. A study of the K_α source with laser parameters such as energy and pulse duration was carried out. The observed K_α X-ray photon flux was $\sim 2.7 \times 10^8$ photons/shot at the laser intensity of $\sim 2.8 \times 10^{17}$ W cm^{-2}. A model was developed to analyze the observed results. The K_α radiation was coupled to a polycapillary collimator to generate a collimated low divergence (0.8 mrad) X-ray beam. Such sources are useful for time-resolved X-ray diffraction and imaging studies.

Keywords: X-ray diffraction; X-ray optics; X-ray sources from laser–plasma interactions

1. INTRODUCTION

The characteristic K_α radiation generated by the interaction of intense, ultra-short laser pulses with solids has unique properties such as, narrow spectral band width and ultra-short pulse duration (<ps) (Zamponi *et al.*, 2010), which makes it suitable for time-resolved X-ray diffraction (TXRD) studies (Sokolowski-Tinten & von der Linde, 2004; Zamponi *et al.*, 2010; Freyer *et al.*, 2013) with high temporal and spatial resolution. Laser–plasma X-ray source also offers high peak brightness and quasi-spectral tuning through the use of various target materials (Z). Other sources such as synchrotron radiation sources can provide X-ray radiation with high average flux (Pfeifer *et al.*, 2006). However, such sources require very large facility and high operating cost. On the other hand, ultra-short pulse duration laser–plasma X-ray sources are compact in size and require low operating cost, which makes them economical and compact alternative. In earlier reported studies, K_α X-ray sources with different target materials and designs such as wire target, metal tape, rotating disk, and liquid jet have been reported (Zhavoronkov *et al.*, 2004; Serbanescu *et al.*, 2007; Chakera *et al.*, 2008; Iqbal *et al.*, 2013; Miaja-Avila *et al.*, 2015). Wire target of different materials are easily available and low-cost in comparison with other target design.

For the practical applications, it is desirable that laser–plasma based K_α X-ray source should have narrow spectral band width, large photon flux, and low bremsstrahlung X-ray noise. In order to maximize the K_α X-ray yield, one should optimize the laser–target interaction parameters such as laser intensity and fluence (Reich *et al.*, 2000, 2001; Curcio *et al.*, 2016). Optimization of laser intensity can be done by changing the laser focal position on the target, by varying the laser energy or laser pulse duration (Arora *et al.*, 2014*b*). Optimization of laser intensity by offsetting the target leads to larger X-ray source size that limits the angular resolution in X-ray diffraction (XRD) studies.

Laser–plasma X-ray source emits in 2π solid angle; therefore it is desirable to collect the emission in order to increase the X-ray flux on the sample under study. Different types of X-ray optics viz. crystal optics, multilayer optics, and polycapillary optics are used for this purpose (Missalla *et al.*, 1999; Bargheer *et al.*, 2005; Shymanovich *et al.*, 2008). Depending on experimental requirement various properties of different optics are useful. Crystal optics provides high spectral purity with small focal spot size, whereas multilayer provides large number of photons per second per mm^2 with small focal spot size (Bargheer *et al.*, 2005). The polycapillary lens provides high X-ray output flux on the sample with moderate focal spot size, whereas polycapillary collimator

*Address correspondence and reprint requests to: R. Rathore, Laser Plasma Section, Raja Ramanna Centre for Advanced Technology, Indore 452013 MP, India. E-mail: ranjana@rrcat.gov.in

provides low divergence and high flux at the sample. The collimated X-ray beam can be transported to large distances, such that the test sample can be placed with higher flexibility (Dorchies *et al.*, 2015). Collimated X-ray beam is useful in various applications such as large area wafer analysis and large area powder diffraction analysis as they give large footprint resulting in much improved particle size distribution statistics and insensitivity of the target placement (Macdonald & Gibson, 2003). The collimated beam also results in higher resolution and contrast in medical imaging (Sugiro *et al.*, 2004). Polycapillary optics contains bundles of thousands of capillary channels. These channels are fused together and bent into tapered shape such that all capillaries are oriented toward the focus, or become parallel to each other (Rath *et al.*, 1998). The X-ray propagates through the channels by total external reflection principle and transmits through it if they enter below the critical angle (~0.2° at 8 keV) (Kumakhov & Komarov, 1990; Rath *et al.*, 1998; Gao & Ponomarev, 2003). In earlier studies, it was observed that the propagation of the X-rays through capillary channels of varying length results in sub-picosecond temporal broadening of X-ray pulse (Tomov *et al.*, 2004). Apart from collecting the X-rays, the energy selectivity of polycapillary optics can filter the undesirable bremsstrahlung X-rays, which exists with the K_α radiation. The hot electrons generated during the laser–plasma interaction can also generate bremsstrahlung radiation from nearby places such as target holder and mounts, etc. This radiation can also couple with the signal and appears as noise. The position sensitivity of polycapillary optics can remove this bremsstrahlung noise effectively. This is highly desirable for various applications viz. phase contrast imaging and X-ray diffraction studies.

In this paper, we report development and parametric characterization of low noise collimated ultra-short K_α X-ray source. The K_α X-ray source is generated by the interaction of 45 fs ultra-short Ti:sapphire laser pulse with Cu wire target. A parametric study of the K_α source such as variation of photon flux and source size with laser parameters, that is, energy and pulse duration was performed and the results are then analyzed using a numerical model. It was observed that the K_α flux increases with the increase in laser energy (fluence) and the maximum observed flux was $\sim 2.7 \times 10^8$ photons per shot at maximum laser intensity of $\sim 2.8 \times 10^{17}$ W cm^{-2}. On the other hand, the K_α flux shows an optimum pulse duration of ~150 fs at a constant energy of 23 mJ (fluence $\sim 6.8 \times 10^3$ J cm^{-2}). Next, the X-ray source size dependence on laser energy (fluence) and pulse duration was also studied. The X-ray source size increases with laser fluence where as it shows a minimum at an optimum pulse duration of ~500 fs. The K_α radiation was coupled to a polycapillary collimator. The collimated output has a low divergence (0.8 mrad) and low bremsstrahlung background. The parallel X-ray beam can be used in various applications as discussed above (Macdonald & Gibson, 2003; Sugiro *et al.*, 2004). X-ray diffraction patterns from the highly oriented pyrolytic graphite (HOPG) crystal were also recorded using collimated and diverging X-ray beams. The comparison of these two diffraction patterns clearly indicates the reduction in background due to rejection of high-energy bremsstrahlung by the polycapillary X-ray optics.

2. EXPERIMENTAL SET UP

The experiment was carried out on 10 TW, Ti:sapphire laser system delivering up to 70 mJ energy in 45 fs [full width at half maximum (FWHM)] laser pulses at 10 Hz repetition rate. The experimental setup is shown in Figure 1. The laser beam was focused using $f/4$ off-axis parabolic (OAP) mirror on a moving Cu wire target of 300 μm diameter to generate Cu K_α radiation. The measured focal spot sizes (FWHM) in horizontal and vertical directions were ~19 and ~11 μm respectively. The p-polarized laser light was incident on the wire target at an angle of ~45° from target normal. The wire target was moved with a speed of ~1 mm s^{-1}, which was sufficient to provide fresh surface at each laser shot operating at 10 Hz. In the direction of the laser beam propagation, the observed shift of the wire around its mean position was <5 μm, which was smaller than the depth of focus (~120 μm) of the OAP. In order to protect OAP from the plasma debris of the wire target, a fused silica window was placed between OAP and wire target assembly. Laser transmission in the fused silica window was ~90%. It may be noted here that ~65% of the laser energy reaches on the target due to losses from folding mirrors, OAP and fused silica window. The energy shown in the figures is actual energy on target.

The X-ray spectrum was recorded on an X-ray charged-coupled device (CCD) camera in a dispersionless geometry, operating in a single photon counting mode (Arora *et al.*, 2013). To avoid the secondary X-ray emission generated by fast electrons, a magnetic field of ~300 Gauss was applied between the X-ray source and X-ray CCD camera. X-ray filters (5-μm thick Al and 7-μm thick Cu) were mounted in front of X-ray CCD to select X-ray energy range of 6–9 keV. From the recorded spectrum, K_α conversion was derived by taking into account the quantum efficiency

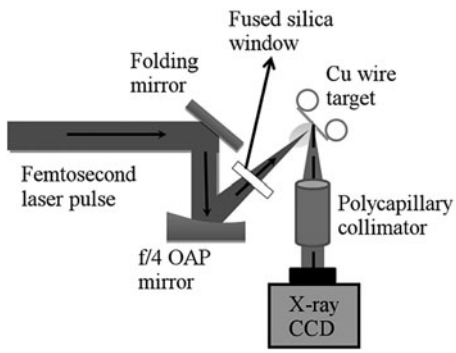

Fig. 1. Schematic representation of experimental setup. The X-ray CCD was used as dispersionless spectrograph when polycapillary collimator was not installed.

https://doi.org/10.1017/S026303461700043X Published online by Cambridge University Press

(17%) of the X-ray CCD detector and the X-ray filter transmission at 8 keV. The K_α X-ray flux variation with laser intensity on the target was studied by (a) changing the laser energy (by changing the energy of laser pumps) on the target and (b) by varying the laser pulse duration (by changing the grating separation of pulse compressor).

Polycapillary X-ray collimator (Make: Unisantis, Model no. = UNS1G-5F-130409) of input focal distance 50 mm, input aperture 5.3 mm, and length 58 mm was used to collimate X-rays coming out from the plasma X-ray source. The polycapillary was mounted on a motorized six-axis goniometer stage. The collimated X-rays were detected by the X-ray CCD camera placed at a distance of ~480 mm from the output end of the collimator. These X-rays were used to record diffraction pattern from HOPG crystal placed outside the vacuum chamber. The X-rays were taken out of the vacuum chamber through a kapton window of 25 μm thickness.

3. RESULT AND DISCUSSION

Single shot X-ray spectrum recorded with dispersionless spectrograph is shown in Figure 2. The spectrum shows Cu K_α (8.05 keV) and K_β (8.9 keV) lines over-riding on a bremsstrahlung background. The K_α X-ray yield is obtained by integrating it over the K_α line width. It was insured that the spectra was recorded in single photon counting mode in order to evaluate the K_α flux correctly. The estimated K_α X-ray photon flux (in 2π Sr) from the recorded spectrum was $\sim 2.7 \times 10^8$ photons per shot at the laser intensity of $\sim 2.8 \times 10^{17}$ W cm^{-2} and X-ray conversion efficiency is estimated to be $\sim 7.6 \times 10^{-6}$ at the above laser intensity. The laser intensity is calculated by assuming Gaussian shape pulse in space and time. The conversion efficiency observed in the present case is comparable with the results reported earlier (Bonvalet *et al.*, 2006; Arora *et al.*, 2014*a*). The variation of K_α photon flux with laser energy (at fixed pulse duration of 45 fs) was also recorded and same is plotted in Figure 3a. The points in the Figure 3a shows the experimental data and the line shows the result on estimation of K_α X-ray flux using theoretical model, which is discussed later. Next, K_α emission is optimized with the laser pulse duration for a constant laser energy of 23 mJ (fluence $\sim 6.8 \times 10^3$ J cm^{-2}) on the target. The laser pulse duration was varied from shortest nominal value of 45 fs to higher duration by changing grating separation of the laser pulse compressor. It was observed that the K_α flux increases first, shows maxima at ~150 fs and then decreases for longer pulse duration as shown in Figure 3b. Similar trend has been reported earlier (Arora *et al.*, 2014*a*). They have observed optimum pulse duration at 250 fs for their experimental condition, which was at higher laser fluence compared with the present case.

A model was developed to understand and estimate the K_α flux. There are several studies available that simulate the process of K_α emission though numerical codes (Eder *et al.*, 2000; Ziener *et al.*, 2002; Limpouch *et al.*, 2004; Gibbon

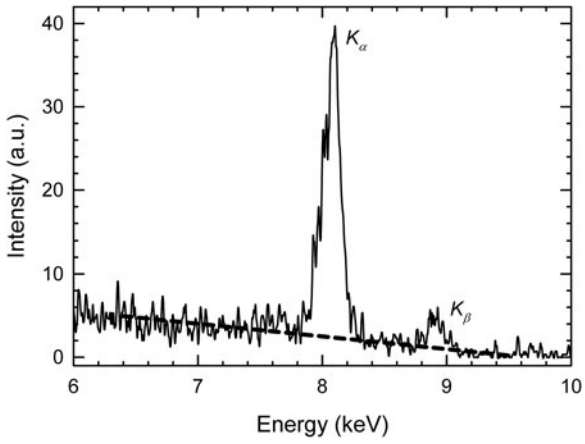

Fig. 2. X-ray spectrum recorded with dispersionless spectrograph. The spectrum shows Cu K_α (8.05 keV) and K_β (8.9 keV) lines overriding on a bremsstrahlung background. The K_α X-ray flux was estimated from the area under the curve. The dashed line indicates the bremsstrahlung background level.

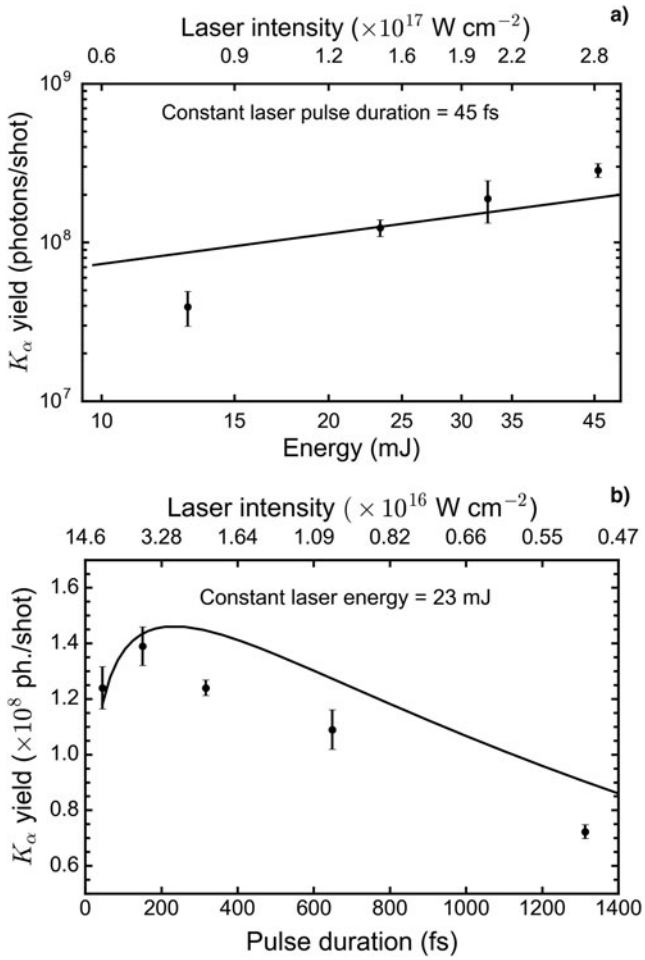

Fig. 3. Variation of K_α X-ray yield (a) with laser energy and (b) with laser pulse duration. Line in the figures show fitted flux distributions from modeling.

https://doi.org/10.1017/S026303461700043X Published online by Cambridge University Press

et al., 2009). These studies mainly use the Monte Carlo or PIC simulations, which is an involved job. Here, we have used a rather simpler numerical approach. The K_α radiation is produced by the interaction of cold solid with hot electrons generated during the interaction of intense ultra-short laser pulse with solid target. However, usually the ultra-short laser pulses have amplified spontaneous emission (ASE) pedestal pre-pulse extending up-to several nanoseconds. When such laser pulse interacts with the target, the ASE pedestal generates pre-plasma extending over several tens of microns. This pre-plasma affects the K_α generation in two ways: first the hot electrons lose their energy in the pre-plasma as they pass though it and a fraction of the generated K_α photons by the interaction of these hot electrons with cold solid also get absorbed in this pre-plasma. However, controlled generation of the pre-plasma can also improve the K_α conversion efficiency (Ziener *et al.*, 2002; Lu *et al.*, 2009). In order to correctly estimate the generated K_α flux, one must take this pre-plasma into account. We have recorded the ASE pedestal using a fast photodiode (MRD 500). The ASE contrast can be controlled by adjusting the switching time of the laser Pockels cells. Under best conditions, the ASE pedestal has ~1% of the laser energy and extended over ~3 ns. The intensity profile of ASE pedestal was used to simulate the density profile of the pre-plasma using a one-dimensional (1D) hydrodynamic code (Helios, 2017). The plasma electron density generated by the laser ASE pedestal as calculated from the 1D hydrodynamic code (Helios, 2017) is shown in Figure 4. Figure 4 inset shows the laser ASE pedestal profile as recorded from photo-diode. Next, we have estimated the temperature of the hot electrons generated in laser solid interaction from earlier works (Beg *et al.*, 1997; Reich *et al.*, 2000; Rao *et al.*, 2012). The experimental and numerical estimations of the hot electron temperature indicate that the hot electron temperature scales with laser intensity as $I^{(0.3–0.6)}$. This scaling is estimated for constant pulse duration and variable laser energy. Here, we have taken the scaling given by Rao *et al.* (2012) ($I^{2/3}$), who have used same laser system in their study. It may be noted here that for the wide range of the laser intensity, the laser energy coupling to hot electrons remains roughly constant (Reich *et al.*, 2000). However, same temperature scaling may not be used while we change the laser pulse duration, as several factors such as laser energy coupling and interaction phenomena may change with laser pulse duration. In order to overcome these unknown factors, we have used the results of Rao *et al.*, where the electron temperature was studied as a function of laser pulse duration. The scaling of hot electron temperature with laser pulse duration was calculated using the results of Rao *et al.*, as $\sim I^{1/3}$. The final expressions of hot electron temperature scaling with laser intensity in both cases can be written as

$$T_{\rm hot}(E) \propto (I)^{2/3} \quad \text{and} \quad T_{\rm hot}(\tau) \propto (I)^{1/3}, \tag{1}$$

where I, $T_{\rm hot}(E)$, and $T_{\rm hot}$ (τ) are laser intensity, hot electron temperatures as a function of laser energy, and laser pulse duration respectively. It may be noted here that in the case of K_α yield with laser energy, different hot electron temperature models give similar results. However, K_α yield with laser pulse duration would strongly depend on different hot electron temperature models. Stronger intensity scaling of hot electron temperature with the laser intensity decreases the K_α flux rapidly with the increase in laser pulse duration. It is assumed that these hot electrons have a Maxwell–Boltzmann distribution at their corresponding hot electron temperature.

$$n = n_0 \sqrt{\frac{E}{kT_{\rm hot}}} \exp\left(-\frac{E}{kT_{\rm hot}}\right), \tag{2}$$

where the value of n_0 can be estimated from the laser energy coupled into hot electrons. In the case of ultra-short pulses focused at normal incidence ~5–10% of the incident laser energy is coupled to the plasma (Price *et al.*, 1995), in other study by Reich *et al.* (2000) ~40–60% laser energy is coupled to the hot electrons. However, our present model can reproduce the experimental results by assuming ~2% coupling of the incident laser energy to the hot electrons. Increasing/decreasing the energy coupling into hot electrons does not change the shape/scaling of the modeled graphs, but merely leads to the change in the flux. The main mechanism involved in the laser-hot electron energy coupling is resonance absorption. In our experimental conditions, where pre-plasma scale length is relatively long (see Figure 4), ~45° incidence angle is far from ideal for efficient resonance absorption. Low incidence angle will be required for efficient resonance absorption. However, we have placed the wire at ~45° to avoid back-reflection and to reduce debris deposition on the beam optics. This might be one of the reasons of the weaker coupling of laser energy into hot electrons (Gibbon, 2005). Since the electron temperature scaling with laser pulse duration takes into account the variation of laser energy coupling into hot electrons and any change in interaction mechanisms, etc. Hence, we can now take constant

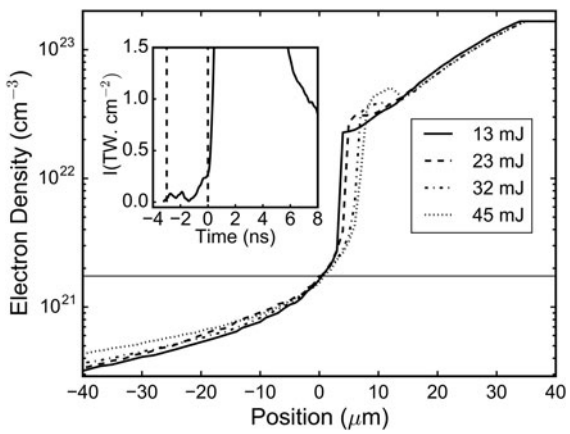

Fig. 4. Simulated electron density profile, generated by the interaction of pre-pulse with the target, using 1D hydrodynamic code (Helios, 2017) at different incident laser energies. The inset shows the ASE pedestal profile recorded by photo-diode (MRD 500) at 45 mJ laser energy.

https://doi.org/10.1017/S026303461700043X Published online by Cambridge University Press

coupling (2%) in this case too. The simulated hot electron distribution as a function of laser energy (at constant pulse duration of 45 fs) and pulse duration (at constant laser energy of 23 mJ) can be seen in Figure 5a and 5b respectively. Upon increasing the laser energy at constant pulse duration, both the laser intensity and the coupled energy to hot electrons increases, which in turn increases the number and temperature of the hot electrons. On the other hand, if we increase the laser pulse duration while keeping the laser energy (fluence) constant, the hot electron temperature decreases but the coupled laser energy into the hot electrons remains the same. As a result the number of the hot electrons increases since the coupled energy is now being distributed among lower energy hot electrons.

Hot electrons generated during laser–matter interaction, traveled first through the pre-plasma and then in the cold solid. The interaction of hot electrons with cold solid generates the K_α radiation. As the hot electrons propagate through the matter, they lose their energy. The energy loss of the electrons depends on the stopping power (energy dependent), and density of the medium. The loss of the electron energy as they propagate through pre-plasma and cold solid was calculated for whole electron distribution at each simulation step of 0.1 μm using electron stopping powers from NIST database (NIST, 2017). The number of K_α photons is estimated from the K_α generation cross-section given by Green & Cosslett (1961)

$$\sigma_k(\mathrm{cm}^2) = 7.92 \times 10^{-20} \frac{\ln(U_k)}{E_k^2(\mathrm{keV})U_k}, \quad (3)$$

Where U_k is the ratio of the electron energy (E) to the K-shell binding energy (E_k). It can be seen from Eq. (3), that the optimum hot electron energy for the generation of the K_α photons is ~25 keV, which is ~3 × the K_α photon energy. When this energy dependent cross-section is multiplied by the electron distribution and the number of the copper atoms in the volume of one simulation step, we will get the K_α photons generated at that simulation step. These K_α photons travel through, solid and pre-plasma, and then reach the detector. We have calculated the number of transmitted photons using positional densities of pre-plasma and solid, and mass absorption cross-section (CXRO, 2017). The addition of these transmitted K_α photons, generated over all simulation steps gives us total number of detected K_α photons for one set of laser parameters. Iterating this process for several laser energies and pulse durations gives us the distribution of generated K_α photons with these parameters as shown in Figure 3a and 3b respectively. These results are matching reasonably well with the observed K_α photon flux. We have compared the total number of K_α photons with the number of atoms present in the interaction volume (i.e. laser focal area × nominal electron range), it turned out that the number of K_α photons is $<10^{-4}$ times the total number of atoms in focal volume.

The other important parameter of the K_α source is its source size as it governs the resolution in X-ray diffraction study and phase contrast imaging. The dependence of K_α source size on the laser parameters was studied using knife edge technique (Fourmaux & Kieffer, 2016). The magnification of the knife edge setup was ~7.5. A knife edge profile at laser intensity $\sim 2.2 \times 10^{17}$ W cm^{-2} is shown in Figure 6 and the derivative of the same gives the X-ray source size

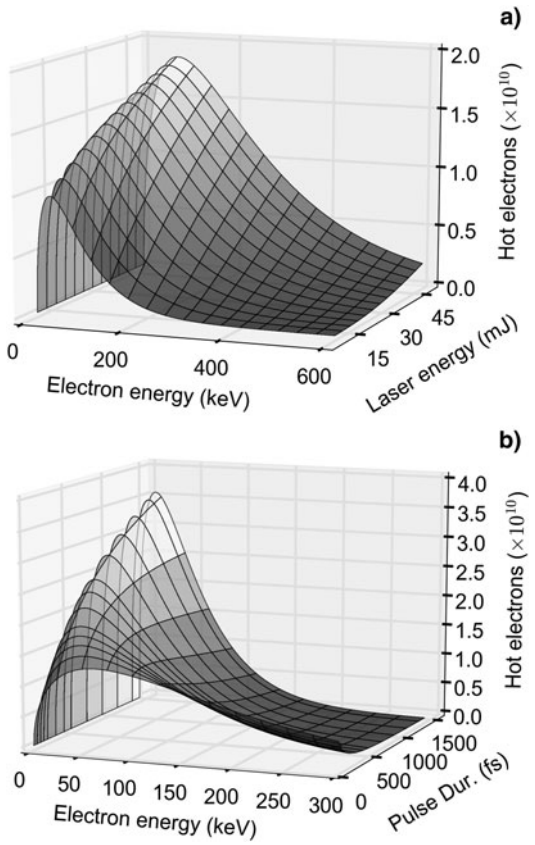

Fig. 5. Simulated hot electron distributions (a) with laser energy at fixed pulse duration of 45 fs and (b) with laser pulse duration at constant laser energy of 23 mJ (fluence $\sim 6.8 \times 10^3$ J cm^{-2}).

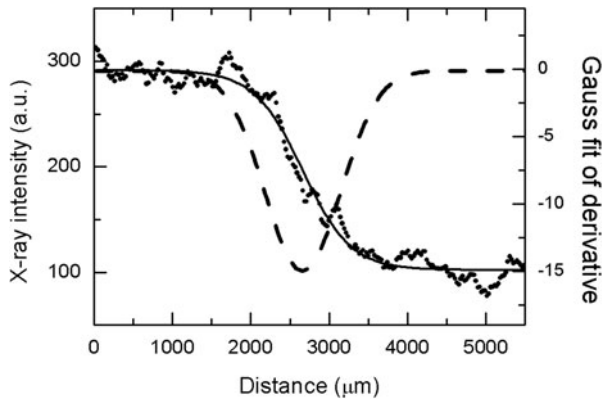

Fig. 6. The knife edge intensity profile of the X-ray source (circles) with error function fit (solid line) and Gauss fit of its first derivative (dashed line). It shows a source size of ~155 μm, recorded at laser intensity of 2.2×10^{17} W cm^{-2}.

https://doi.org/10.1017/S026303461700043X Published online by Cambridge University Press

~155 μm (FWHM) in horizontal direction. The variation of X-ray source size with laser energy and pulse duration was studied. It was observed that for a constant pulse duration (45 fs) with increasing laser energy, source size increases and the same is shown in Figure 7a. Variation of the source size with laser pulse duration for a constant energy of 36 mJ (fluence $\sim 1.1 \times 10^4$ J cm^{-2}) is shown in Figure 7b. It may be noted that the X-ray source size first decreases sharply to a minimum at ~500 fs. With the further increase in laser pulse duration the X-ray source size again started increasing slowly.

Interaction of ultra-short laser with the solid target generates hot electrons with a divergence that depends on various laser–plasma interaction parameters. The K_α photons are generated by these hot electrons along their propagation in the cold solid. Thus, the K_α X-ray source size is similar to the average transverse size of the hot electrons in the cold medium. The presence of pre-plasma increases the transverse size of the hot electrons generated at the critical density surface, hence the observed X-ray source size was significantly larger than the laser focal spot size (Eder *et al.*, 2000). With the increase in laser pulse duration, the laser intensity decreases which in turn decrease the temperature/range of the hot electrons. As the hot electron range decreases, the diverging hot electrons penetrate less in the medium, hence the final transverse size of the hot electrons also decreases, which in turn decreases the K_α source size. After initial increase in laser pulse duration, the hot electron range becomes sufficiently less, such that K_α photons come essentially from the surface of the target. Hence, further increase in laser pulse duration does not decrease the K_α source size. However, the increase in the divergence of hot electrons with laser pulse duration (Mandal *et al.*, 2015) may increase the K_α source size with further increase in laser pulse duration. More experimental and simulation data are required to firmly establish this fact. In similar line, as the laser energy is increased, the hot electron temperature/range increases. The K_α photons are generated deeper inside the material resulting in the increase in K_α source size.

As discussed above, the bremsstrahlung background generated during the laser–plasma interaction acts as noise in the K_α X-ray source and not desirable in various applications. Further, it is also important to collect the K_α radiation from the laser–plasma point X-ray source, which emits in 2π solid angle and transport it to the sample for better flux. These requirements may be achieved by collecting and collimating the X-rays emitting from the point X-ray source using polycapillary optics.

The X-rays were collected by a polycapillary collimator placed at a distance of 50 mm from the source. The image of the collimated X-ray beam recorded on the X-ray CCD along with its horizontal and vertical profiles is shown in Figure 8. The X-ray flux through polycapillary is optimized by precisely aligning its position and angle with respect to X-ray source using goniometer. The observed horizontal and vertical FWHM sizes of the collimated beam were 2.83 and 2.76 mm respectively. A 25 μm thick kapton window was used to transmit the collimated X-ray output from the vacuum chamber. The divergence of the collimated beam was measured by recording it on X-ray image plate

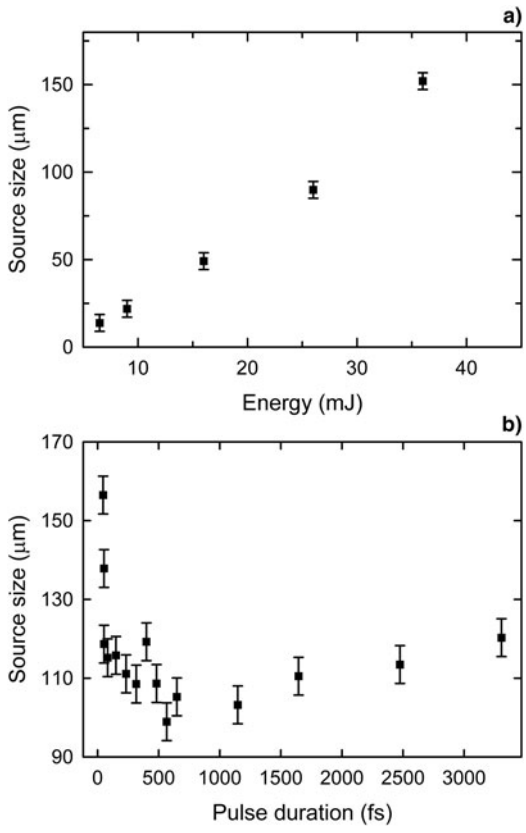

Fig. 7. Variation of X-ray source size (a) with laser energy at fixed pulse duration of 45 fs and (b) with laser pulse duration at fixed laser energy of 36 mJ (fluence $\sim 1.1 \times 10^4$ J cm^{-2}). Source size shows monotonic increase with laser energy, whereas with increase in pulse duration the source size first decreases and then it increases slowly.

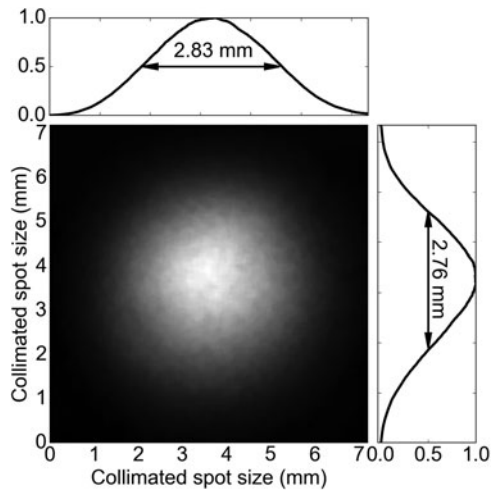

Fig. 8. Collimated X-ray beam profile.

https://doi.org/10.1017/S026303461700043X Published online by Cambridge University Press

detector at two different positions viz. 410 mm and 1850 mm from the exit of the collimator lens and the divergence was measured to be ~0.8 mrad.

The diffraction pattern of collimated X-rays taken from HOPG crystal spectrograph is shown in Figure 9a and the inset shows the photograph of the diffraction pattern. The HOPG crystal was chosen in view of its large mosaicity of 4.7°. The mosaicity of the HOPG crystal makes it easier to align with parallel X-ray beam, since to get the diffracted output from the single crystal, one needs to align the crystal with an accuracy of its rocking curve. The diffracted profile of the X-rays shows a clean spectrum. On the other hand, the diffracted X-ray spectrum of diverging beam from the HOPG crystal (Fig. 9b) as well as the spectrum taken from dispersionless spectrograph (Fig. 2) shows the significant presence of bremsstrahlung radiation background. As discussed earlier, the position and wavelength selectivity of the polycapillary optics resulted in the reduction of the bremsstrahlung noise. Unlike the diverging X-ray source, where the diffracted profile is governed by the rocking curve of the crystal (Fig. 9b), a parallel beam will diffract as a parallel beam and should create a circular profile on the detector. However, in our case we have seen an oblong profile and both K_α and K_β lines (Fig. 9a). It may be due to slight curvature in the HOPG crystal.

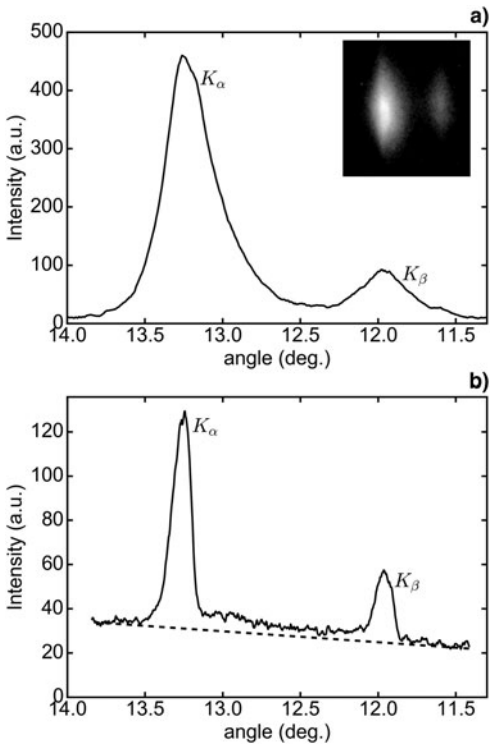

Fig. 9. The diffraction patterns from HOPG crystal (a) using collimated X-ray beam. The inset shows the image of diffracted beam and (b) using diverging X-ray beam. The dashed line indicates the bremsstrahlung background. It is evident that the bremsstrahlung noise is decreased substantially in Fig. 9a.

4. CONCLUSION

We have performed parametric characterization of ultra-short K_α X-ray source generated by the interaction of 45 fs Ti:sapphire laser pulse with Cu wire target. The K_α flux variation with laser energy and pulse duration was studied. It was observed that K_α flux increases monotonically with laser energy, on the other hand, K_α flux maximized for optimum pulse duration of ~150 fs. A numerical model was developed to analyze the observed results. The simulated results agreed reasonably well with the experimental observations. The K_α source size variation with laser energy and pulse duration was also studied. The source size increases monotonically with the laser energy; however, it shows a minimum for laser pulse duration of ~500 fs. This K_α radiation is coupled to a polycapillary collimator to generate a collimated low divergence (0.8 mrad) X-ray beam. The collimated X-ray beam can be transported at larger distances for better X-ray flux and flexibility in sample placement. This X-ray beam was diffracted from a HOPG crystal. The diffracted profile of the collimated beam shows significant reduction in the bremsstrahlung noise compared with that from without polycapillary optics.

ACKNOWLEDGMENTS

The authors would like to acknowledge Shri R.A. Joshi and Shri R. K. Bhat for laser operation, Shri S. Sebastin, Shri R.P. Kushwaha and Shri K.C. Parmar for mechanical support during the experiment. We thank Shri A. Padiyar for designing wire target assembly. We also thank laser electronic support division, RRCAT for their support in providing power supplies.

REFERENCES

Arora, V., Naik, P.A., Chakera, J.A., Bagchi, S., Tayyab, M. & Gupta, P.D. (2014*a*). Study of 1–8 keV K-α X-ray emission from high intensity femtosecond laser produced plasma. *AIP Adv*. **4**, 047106.

Arora, V., Naik, P.A., Chakravarty, U., Singhal, H., Rao, B.S., Chakera, J.A., Singh, M.P. & Gupta, P.D. (2014*b*). A comparative study of the inner-shell and the ionic line radiation from ultra-short laser-produced magnesium plasma. *Phys. Scr*. **89**, 115601.

Arora, V., Vora, H.S., Chakera, J.A., Tayyab, M., Naik, P.A. & Gupta, P.D. (2013). Dispersion-less spectrograph for absolute measurement of multi keV X-ray flux from high intensity laser produced plasmas. *J. Instrum*. **8**, P01010.

Bargheer, M., Zhavoronkov, N., Bruch, R., Legall, H., Stiel, H., Woerner, M. & Elsaesser, T. (2005). Comparison of focusing optics for femtosecond X-ray diffraction. *Appl. Phys. B* **80**, 715–719.

Beg, F.N., Bell, A.R., Dangor, A.E., Danson, C.N., Fews, A.P., Glinsky, M.E., Hammel, B.A., Lee, P., Norreys, P.A. & Tatarakis, M. (1997). A study of picosecond laser–solid interactions up to 1019 W cm−2. *Phys. Plasmas* **4**, 447–457.

Bonvalet, A., Darmon, A., Lambry, J.-C., Martin, J.-L. & Audebert, P. (2006). 1 kHz tabletop ultrashort hard x-ray source for time-resolved x-ray protein crystallography. *Opt. Lett*. **31**, 2753.

https://doi.org/10.1017/S026303461700043X Published online by Cambridge University Press

Chakera, J.A., Ali, A., Tsui, Y.Y. & Fedosejevs, R. (2008). A continuous kilohertz CuKa source produced by submillijoule femtosecond laser pulses for phase contrast imaging. *Appl. Phys. Lett*. **93**, 261501.

Curcio, A., Anania, M., Bisesto, F.G., Faenov, A., Ferrario, M., Galletti, M., Giulietti, D., Kodama, R., Petrarca, M., Pikuz, T. & Zigler, A. (2016). Characterization of X-ray radiation from solid Sn target irradiated by femtosecond laser pulses in the presence of air plasma sparks. *Laser Part. Beams* **34**, 533–538.

CXRO, (2017). Filter Transmission. http://henke.lbl.gov/optical_constants/filter2.html.

Dorchies, F., Fedorov, N. & Lecherbourg, L. (2015). Experimental station for laser-based picosecond time-resolved X-ray absorption near-edge spectroscopy. *Rev. Sci. Instrum*. **86**, 073106.

Eder, D.C., Pretzler, G., Fill, E., Eidmann, K. & Saemann, A. (2000). Spatial characteristics of Kα radiation from weakly relativistic laser plasmas. *Appl. Phys. B* **70**, 211–217.

Fourmaux, S. & Kieffer, J.C. (2016). Laser-based K α X-ray emission characterization using a high contrast ratio and high-power laser system. *Appl. Phys. B* **122**, 1–10.

Freyer, B., Zamponi, F., Juvé, V., Stingl, J., Woerner, M., Elsaesser, T. & Chergui, M. (2013). Ultrafast inter-ionic charge transfer of transition-metal complexes mapped by femtosecond X-ray powder diffraction. *J. Chem. Phys*. **138**, 144504.

Gao, N. & Ponomarev, I.Y. (2003). Polycapillary X-ray optics: manufacturing status, characterization and the future of the technology. *X-Ray Spectrom*. **32**, 186–194.

Gibbon, P. (2005). *Short Pulse Laser Interactions with Matter an Introduction*. London: Imperial College Press.

Gibbon, P., Mašek, M., Teubner, U., Lu, W., Nicoul, M., Shymanovich, U., Tarasevitch, A., Zhou, P., Sokolowski-Tinten, K. & von der Linde, D. (2009). Modelling and optimisation of fs laser-produced Kα sources. *Appl. Phys. A* **96**, 23–31.

Green, M. & Cosslett, V.E. (1961). The efficiency of production of characteristic X-radiation in thick targets of a pure element. *Proc. Phys. Soc*. **78**, 1206.

Helios, v 7.3 (2017). 1-D Radiation-Hydrodynamic Code. http://www.prism-cs.com/Software/Helios/Helios.htm.

Iqbal, M., Urrehman, Z., Im, H., Son, J.G., Seo, O., Stiel, H., Nickles, P.V., Noh, D.Y. & Janulewicz, K.A. (2013). Performance improvement of a Kα source by a high-resolution thin-layer-graphite spectrometer and a polycapillary lens. *Appl. Phys. B* **116**, 305–311.

Kumakhov, M.A. & Komarov, F.F. (1990). Multiple reflection from surface X-ray optics. *Phys. Rep*. **191**, 289–350.

Limpouch, J., Klimo, O., Bína, V. & Kawata, S. (2004). Numerical studies on the ultrashort pulse K-α emission sources based on femtosecond laser-target interactions. *Laser Part. Beams* **22**, 147–156.

Lu, W., Nicoul, M., Shymanovich, U., Tarasevitch, A., Zhou, P., Sokolowski-Tinten, K., von der Linde, D., Mašek, M., Gibbon, P. & Teubner, U. (2009). Optimized K_α X-ray flashes from femtosecond-laser-irradiated foils. *Phys. Rev. E* **80**, 026404.

Macdonald, C.A. & Gibson, W.M. (2003). Applications and advances in polycapillary optics. *X-Ray Spectrom*. 32, 258–268.

Mandal, T., Arora, V., Tayyab, M., Bagchi, S., Rathore, R., Ramakrishna, B., Mukharjee, C., Chakera, J.A., Naik, P.A. & Gupta, P.D. (2015). Study of fast electron transport in thin foil targets irradiated by ultrashort intense laser pulses. *Appl. Phys. B* **119**, 281–286.

Miaja-Avila, L., O'Neil, G.C., Uhlig, J., Cromer, C.L., Dowell, M.L., Jimenez, R., Hoover, A.S., Silverman, K.L. & Ullom, J.N. (2015). Laser plasma X-ray source for ultrafast time-resolved X-ray absorption spectroscopy. *Struct. Dyn*. **2**, 024301.

Missalla, T., Uschmann, I., Förster, E., Jenke, G. & von der Linde, D. (1999). Monochromatic focusing of subpicosecond X-ray pulses in the keV range. *Rev. Sci. Instrum*. **70**, 1288–1299.

NIST, (2017). Stopping Power and Range Tables for Electrons. http://physics.nist.gov/PhysRefData/Star/Text/ESTAR.html.

Pfeifer, T., Spielmann, C. & Gerber, G. (2006). Femtosecond X-ray science. *Rep. Prog. Phys*. **69**, 443.

Price, D.F., More, R.M., Walling, R.S., Guethlein, G., Shepherd, R.L., Stewart, R.E. & White, W.E. (1995). Absorption of ultrashort laser pulses by solid targets heated rapidly to temperatures 1–1000 eV. *Phys. Rev. Lett*. **75**, 252–255.

Rao, B.S., Arora, V., Naik, P.A. & Gupta, P.D. (2012). Study of fast electron jet produced from interaction of intense laser beam with solid target at oblique incidence. *Phys. Plasmas* **19**, 113118.

Rath, B.K., Wang, L., Homan, B.E., Hofmann, F., Gibson, W.M. & MacDonald, C.A. (1998). Measurements and analysis of radiation effects in polycapillary X-ray optics. *J. Appl. Phys*. **83**, 7424–7435.

Reich, Ch., Gibbon, P., Uschmann, I. & Förster, E. (2000). Yield optimization and time structure of femtosecond laser plasma K_α sources. *Phys. Rev. Lett*. **84**, 4846–4849.

Reich, Ch, Gibbon, P., Uschmann, I. & Förster, E. (2001). Numerical studies on the properties of femtosecond laser plasma K_α sources. *Laser Part. Beams* **19**, 147–150.

Serbanescu, C.G., Chakera, J.A. & Fedosejevs, R. (2007). Efficient K_α X-ray source from submillijoule femtosecond laser pulses operated at kilohertz repetition rate. *Rev. Sci. Instrum*. **78**, 103502.

Shymanovich, U., Nicoul, M., Sokolowski-Tinten, K., Tarasevitch, A., Michaelsen, C. & von der Linde, D. (2008). Characterization and comparison of X-ray focusing optics for ultrafast X-ray diffraction experiments. *Appl. Phys. B* **92**, 493–499.

Sokolowski-Tinten, K. & von der Linde, D. (2004). Ultrafast phase transitions and lattice dynamics probed using laser-produced X-ray pulses. *J. Phys. Condens. Matter* **16**, R1517.

Sugiro, F.R., Li, D. & MacDonald, C.A. (2004). Beam collimation with polycapillary X-ray optics for high contrast high resolution monochromatic imaging. *Med. Phys*. **31**, 3288–3297.

Tomov, I.V., Chen, J., Ding, X. & Rentzepis, P.M. (2004). Efficient focusing of hard X-rays generated by femtosecond laser driven plasma. *Chem. Phys. Lett*. **389**, 363–366.

Zamponi, F., Ansari, Z., Woerner, M. & Elsaesser, T. (2010). Femtosecond powder diffraction with a laser-driven hard X-ray source. *Opt. Express* **18**, 947.

Zhavoronkov, N., Gritsai, Y., Korn, G. & Elsaesser, T. (2004). Ultra-short efficient laser-driven hard X-ray source operated at a kHz repetition rate. *Appl. Phys. B* **79**, 663–667.

Ziener, Ch., Uschmann, I., Stobrawa, G., Reich, Ch., Gibbon, P., Feurer, T., Morak, A., Düsterer, S., Schwoerer, H., Förster, E. & Sauerbrey, R. (2002). Optimization of K_α bursts for photon energies between 1.7 and 7 keV produced by femtosecond-laser-produced plasmas of different scale length. *Phys. Rev. E* **65**, 066411.

https://doi.org/10.1017/S026303461700043X Published online by Cambridge University Press